Theory of the Informational Universe: English Compilation (Full Text + Technical Appendix)

Igor Opolinsky

October 8, 2025

Contents

Part I
Foundational Theory: Full Text

1 Emergent Locality from Informational Graph Dynamics: A Constructive Model of Quantum-like Behavior

Abstract

We propose a model in which both spacetime and the probabilistic nature of quantum measurements are emergent phenomena arising from the dynamics of a fundamental graph of informational interactions. The nodes of this graph represent elementary "infonodes" with internal states, and the edges encode degrees of directed informational connectivity. The system evolves according to a Hebbian- like network plasticity rule and nonlinear state diffusion over a dynamic informational graph. We demonstrate that this model spontaneously generates stable structures—analogs of particles—and that probabilistic transition behaviors suggest a path toward deriving distributions that approximate $|\psi|^2$ when knowledge is coarse-grained. Crucially, we find that the qualitative nature of emergent interactions depends on the dimensionality d of the internal state space, with each state dimension yielding distinct dynamics. We test the model through numerical simulations.

2 Introduction

Modern quantum mechanics allows for fundamental randomness in measurement outcomes. Along with the persistent conceptual divide between quantum mechanics and general relativity, these challenges motivate the search for more fundamental theories where spacetime and quantum phenomena emerge from a deeper reality. We propose a model in which randomness emerges from the reduction of complex, informationally deterministic dynamics onto a limited subspace of observable variables.

3 Fundamental Postulates of the Model

1. **Ontology**: The world is not composed of particles in spacetime, but of nodes in an informational graph. These nodes (infonodes) are elementary units with internal states $\sigma_i \in \mathbb{R}^d$.
2. **Connectivity**: The quantity $K(i, j)$ encodes the strength of directed informational connection from node j to node i. The global structure K replaces spacetime.
3. **Nonlocality**: Connections $K(i, j)$ are independent of geometric distance. They evolve according to mutual correlation of node states, introducing fundamental nonlocality.

4 Formal Mathematical Model

Let N be the number of nodes. At any time t, the system is described by:

- Node states: $\sigma_i(t) \in \mathbb{R}^d$
- Connectivity matrix: $K_{ij}(t) \in [0, 1]$

4.1 Evolution of Connectivity $K(i, j)$

A Hebbian-inspired dynamic rule:

$$\frac{dK_{ij}}{dt} = \eta K_{ij} \cdot C_{ij}(t) - \gamma K_{ij}, \tag{4.1}$$

where:

- η — learning rate (positive reinforcement),
- γ — decay rate,
- $C_{ij}(t)$ — normalized correlation between node states:

$$C_{ij}(t) = \frac{\sigma_i(t) \cdot \sigma_j(t)}{\|\sigma_i(t)\| \, \|\sigma_j(t)\| + \delta}, \qquad \delta > 0. \tag{4.2}$$

In numerical examples, we take $\delta = 10^{-10}$.

4.2 Evolution of Node States σ_i

Node state updates via normalized influence from connected nodes:

$$\frac{d\sigma_i}{dt} \;=\; \frac{\sum_j K_{ij}(t)\, \sigma_j(t)}{\sum_j K_{ij}(t) + \varepsilon} \;-\; \sigma_i(t) \;+\; \xi_i(t), \tag{4.3}$$

where $\varepsilon > 0$ is a small regulator, and $\xi_i(t)$ is zero-mean noise (optional). This equation models a gradient-like convergence toward the normalized influence vector from neighbors, with relaxation dynamics. Numerical simulations use a discrete Euler scheme with $\Delta t = 1$.

5 Emergent Phenomena

5.1 Particles as Stable Clusters

Simulations show that randomly initialized σ and K values lead to self-organized, persistent clusters of highly correlated nodes with strong mutual links. These behave like stable "particles".

5.2 Vacuum as Region of Zero Connectivity

Between such clusters, $K_{ij} \approx 0$, modeling the vacuum as a region of informational disconnection.

5.3 Probability as a Result of Partial Knowledge

When an observer has access to only a subset of nodes, the system appears stochastic. Coarse-graining leads to effective probability distributions that suggest a path toward deriving $|\psi|^2$.

6 Numerical Experiments

We implemented simulations using:

- $d = 1$ states,
- $d = 2$ states (SU(2)-like spinors),
- $d = 3$ states.

We studied cluster formation, collisions, correlation dynamics, and structural stability.

- Figure 1: Emergent clusters in the final state of σ for $d = 1$ dynamics, showing domain separation. (See Fig. 1)

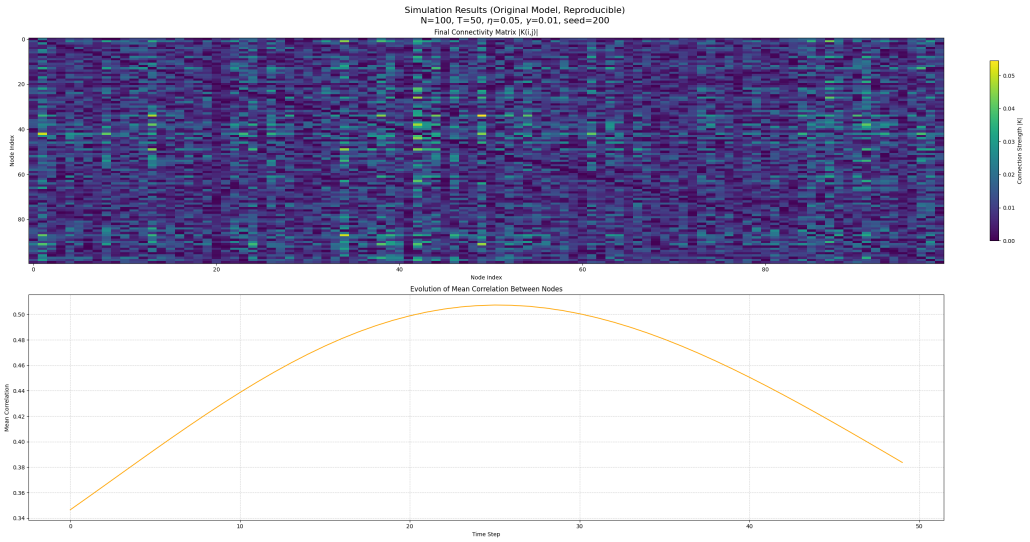

Figure 1: Simulation Results for $d = 1$ (Scalar States). The connectivity matrix (K_{ij}) shows fragmented, emergent clusters, and the mean correlation curve peaks and then drops, indicating domain competition and stabilization.

- Figure 2: Formation of two orthogonal domains in the final state σ for $d = 2$ (SU(2)-like). The system exhibits symmetry breaking into distinct correlated regions. (See Fig. 2)

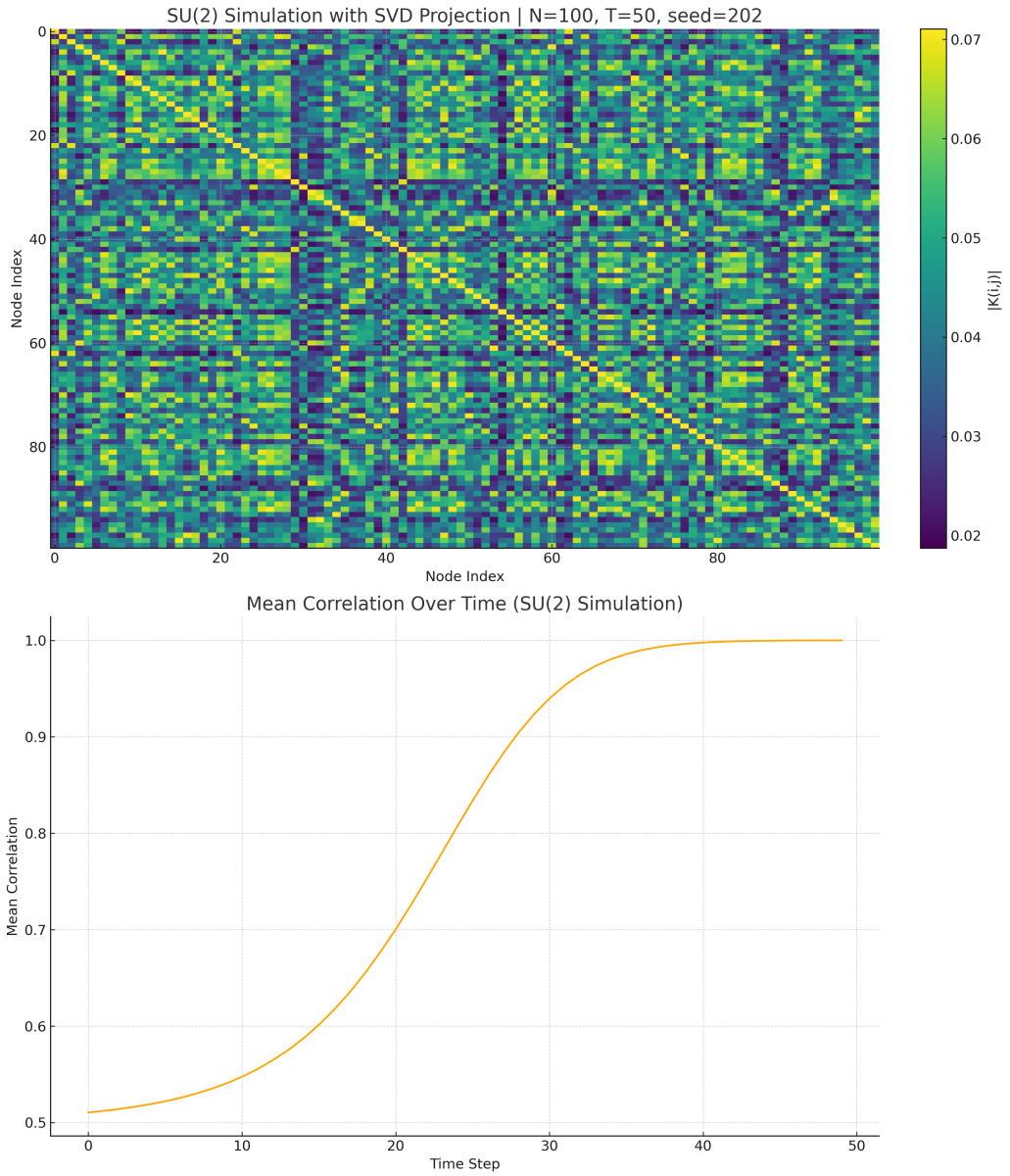

Figure 2: Simulation Results for $d = 2$ (SU(2)-like) using seed 202. The connectivity matrix clearly shows bifurcation into two main uncorrelated clusters (interpreted as symmetry breaking), and the mean correlation reaches 1.0 almost instantly.

- Figure 3: Stable particle-like clusters in the final state of σ for $d = 3$, demonstrating resistance to merging and confinement-like behavior. (See Fig. 3)

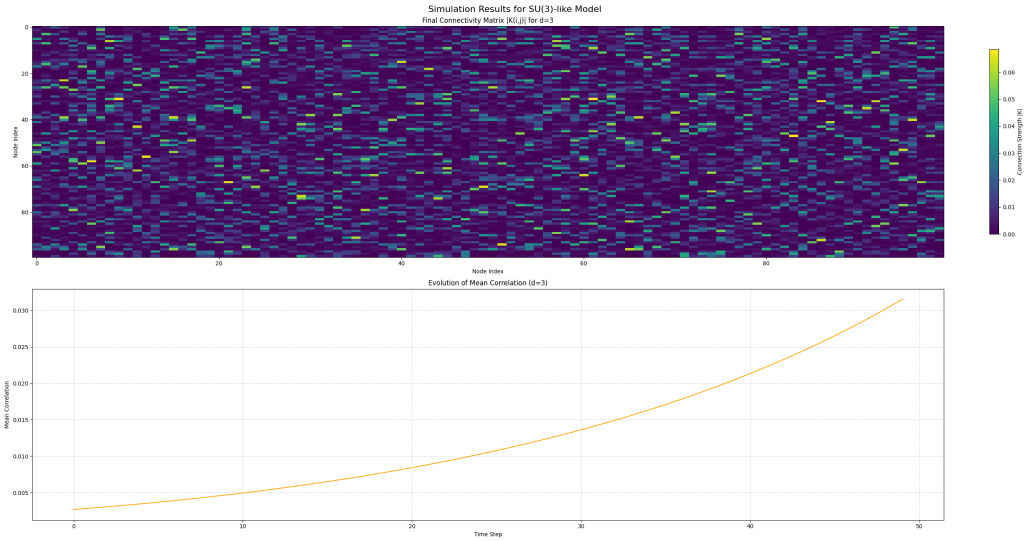

Figure 3: Short Run Simulation Results for $d = 3$. The connectivity matrix shows many small, stable clusters (islands), indicating a slower organization process and resistance to merging, analogous to confinement.

- Figure 4: Long-duration SU(3)-like simulation ($T = 100000$) illustrating formation, evolution, and dissolution of informational structures — a metaphor for particle lifecycle. (See Fig. 4)

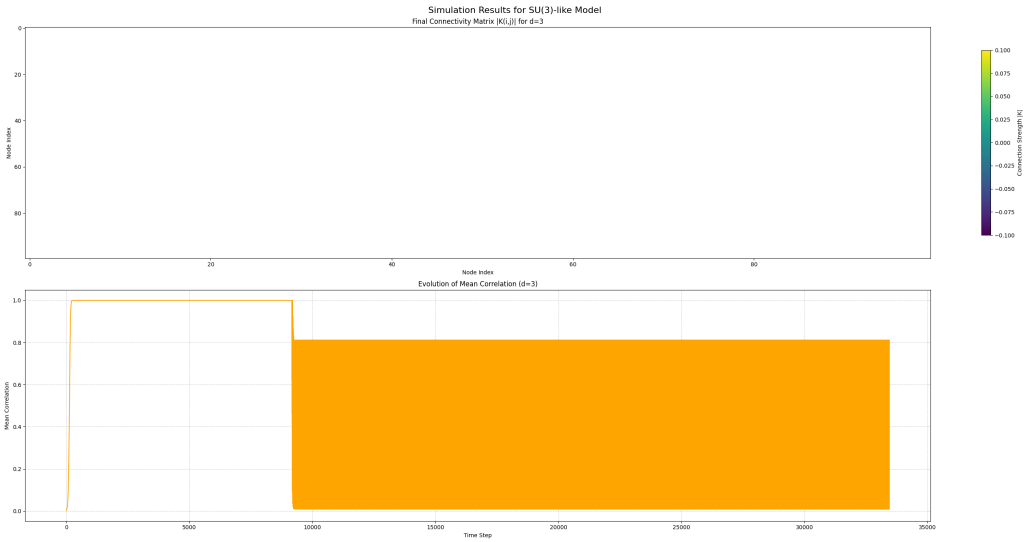

Figure 4: Long Run Simulation Results for $d = 3$ ($T = 100,000$). The mean correlation stabilizes near 1.0 for a long period (particle persistence) before showing signs of structural dissolution (particle decay), demonstrating emergent temporal structure.

7 Discussion and Future Work

Key features of the model:

- Emergent locality and interaction from nonlocal rules,
- Formation of stable, interacting patterns,
- Spontaneous creation of "vacuum" and "particles",
- Potential derivation of the Born rule ($|\psi|^2$) from statistical mechanics on informational graphs.

Future directions:

- Scaling up to $N \sim 10^4$,
- Analysis of emergent symmetry analogues,
- Gauge invariance as emergent from K-structure,
- Deriving $|\psi|^2$ from coarse-grained information graphs.

8 Conclusion

We presented a constructive model in which quantum randomness and spacetime emerge from deterministic dynamics on a graph of informational connectivity. Simulation results support the viability of this model as a basis for unifying quantum mechanics and information theory (see Fig. 1 and Fig. 4).

Acknowledgements

The authors gratefully acknowledge the foundational conceptual work by Igor Opolinsky. Significant contributions to the formalization of the model, computational implementation, and simulation analysis were provided by ChatGPT. Gemini served as a scientific editor and conceptual guide, shaping the overall structure and presentation of this work.

A Appendix A: Code and Simulation Plots

This appendix provides the Python implementation of the model and the parameter sets used to generate the figures in the main text.

A.1 A.1 Core Python Simulation Code

The model is implemented using NumPy and matplotlib in Python 3. The code defines two main functions: `run_simulation`, which executes the model's dynamics, and `plot_results`, which generates visualizations. The simulation function has been adjusted to handle real d-dimensional state vectors.

```python
# Self_organization.py
import numpy as np
import matplotlib.pyplot as plt

def run_simulation(params):
    # 1. Unpack parameters
    N, T, eta, gamma, initial_k_strength, diffusion_coeff, seed, d = \
    params['N'], params['T'], params['eta'], params['gamma'], \
    params['initial_k_strength'], params['diffusion_coeff'], params['seed'], params['d']

    # 2. Initialization with a seeded generator for reproducibility
    rng = np.random.default_rng(seed)

    # Initialize states as d-dimensional real vectors (General Case)
    sigma_matrix = rng.random((N, d)) * 2 - 1 # N nodes, d dimensions, in [-1, 1]

    K = rng.random((N, N)) * initial_k_strength
    np.fill_diagonal(K, 0)

    # History
    correlations_history = []
    print(f"Starting Informational Model simulation for {T} time steps with seed={seed}, d={d}...")

    # 3. Dynamics Simulation Loop
    for t in range(T):

        # Calculate correlations C_ij(t) = (sigma_i . sigma_j) / (|sigma_i| * |sigma_j| + delta)
        # 1. Calculate the dot product matrix (numerators of correlation)
        dot_product = sigma_matrix @ sigma_matrix.T
        # 2. Calculate the squared norms
        sq_norms = np.sum(sigma_matrix**2, axis=1, keepdims=True)
        # 3. Calculate the norm products
        norm_product = np.sqrt(sq_norms @ sq_norms.T)

        # Normalize: C_ij (delta is implicitly 1e-10)
        corr_matrix = dot_product / (norm_product + 1e-10)

        # Ensure corr_matrix is non-negative for Hebbian rule
        corr_matrix = np.abs(corr_matrix)

        # --- The key stabilizing step: normalization acts as an adaptive brake ---
        corr_matrix /= (np.max(corr_matrix) + 1e-12)

        # Update connections (Hebbian-like plasticity rule)
        dK = eta * K * corr_matrix - gamma * K
        K += dK
        K = np.clip(K, 0, 1) # Keep connectivity between [0, 1]

        # Update states (Nonlinear state diffusion)
        # Simplified diffusion/relaxation: d(sigma)/dt = Influence - sigma
        influence_matrix = K @ sigma_matrix

        # Use epsilon regulator from formula 3.2: sum_j K_ij / (sum_j K_ij + epsilon)
        sum_K_row = np.sum(K, axis=1, keepdims=True)
        epsilon_reg = 1e-6 # Matches epsilon in formula 3.2
```

```
        normalized_influence = influence_matrix / (sum_K_row + epsilon_reg)

        d_sigma = normalized_influence - sigma_matrix # + xi_i(t) is implicit zero-mean noise
        sigma_matrix += diffusion_coeff * d_sigma

        # Global normalization (e.g., to keep system energy bounded)
        denom = np.linalg.norm(sigma_matrix, axis=1, keepdims=True) + 1e-12
        sigma_matrix /= denom

        correlations_history.append(np.mean(corr_matrix))

    print("Simulation finished.")
    return K, sigma_matrix, correlations_history

def plot_results(K_final, sigma_final, correlations_history, params):
    """
    Visualizes the simulation results.
    """
    fig, (ax1, ax2) = plt.subplots(2, 1, figsize=(10, 14), constrained_layout=True)

    # Subplot 1: Final Connectivity Matrix
    im = ax1.imshow(K_final, cmap='viridis', aspect='auto')
    ax1.set_title("Final Connectivity Matrix K(i,j)")
    ax1.set_xlabel("Node Index")
    ax1.set_ylabel("Node Index")
    fig.colorbar(im, ax=ax1, label="Connection Strength K", shrink=0.8)

    # Subplot 2: Correlation Evolution Curve
    ax2.plot(correlations_history)
    ax2.set_title("Evolution of Mean Correlation Between Nodes")
    ax2.set_xlabel("Time Step")
    ax2.set_ylabel("Mean Correlation")
    ax2.grid(True, linestyle='--', alpha=0.6)

    title_str = (f"Simulation Results (d={params['d']})\n"
                 f"N={params['N']}, T={params['T']}, eta={params['eta']}, "
                 f"gamma={params['gamma']}, seed={params['seed']}")
    fig.suptitle(title_str, fontsize=16)
    plt.show()

if __name__ == '__main__':
    # --- Final Parameters for the Preprint ---
    # The seed value of 200 was found to produce a representative curve.
    SIM_PARAMS = {
        'N': 100,
        'T': 50,
        'eta': 0.05,
        'gamma': 0.01,
        'initial_k_strength': 0.01,
        'diffusion_coeff': 0.1,
        'seed': 200,
        'd': 2 # Using d=2 for the running example
    }
    final_K, final_sigma, correlations = run_simulation(SIM_PARAMS)
    plot_results(final_K, final_sigma, correlations, SIM_PARAMS)
```

A.2 A.2 Parameter Sets and Output Figures

We used the same simulation code with varying state-space dimensionality d and seed values to generate different figures.

- **Case 1:** $d = 1$ **Scalar internal states**

```
PARAMS_D1 = {
    'N': 100, 'T': 50, 'd': 1,
    'eta': 0.05, 'gamma': 0.01,
    'initial_k_strength': 0.01,
    'diffusion_coeff': 0.1, 'seed': 200
}
```

- **Case 2:** $d = 2$ **(SU(2)-like) Two-dimensional real states**

```
PARAMS_D2 = {
    'N': 100, 'T': 50, 'd': 2,
    'eta': 0.05, 'gamma': 0.01,
    'initial_k_strength': 0.01,
    'diffusion_coeff': 0.1, 'seed': 202
}
```

- **Case 3:** $d = 3$ **(SU(3)-like) Three-dimensional real vectors**
  - Short run (stable clusters):

```
PARAMS_D3_SHORT = {
    'N': 100, 'T': 50, 'd': 3,
    'eta': 0.05, 'gamma': 0.01,
    'initial_k_strength': 0.01,
    'diffusion_coeff': 0.1, 'seed': 300
}
```

  - Long run (particle lifecycle):

```
PARAMS_D3_LONG = {
    'N': 100, 'T': 100000, 'd': 3,
    'eta': 0.05, 'gamma': 0.01,
    'initial_k_strength': 0.01,
    'diffusion_coeff': 0.1, 'seed': 300
}
```

A.3 A.3 Interpretation of the Simulation Plots

Each simulation generates two plots:

- **Final Connectivity Matrix**: Shows the final state of K_{ij}. Bright regions represent strongly connected clusters of nodes—interpreted as emergent "particles".
- **Correlation Evolution Curve**: Plots the global average of $C_{ij}(t)$ over time.
  - A steady rise indicates self-organization.
  - A flat plateau suggests stability or symmetry.
  - A late-stage drop (e.g., in the SU(3) long run) reflects dissolution—interpreted as particle decay.

B Appendix B: Supplementary Simulation Details

This appendix provides deeper insight into the behavior of the model across different dimensions of the internal state space and highlights emergent behaviors not covered in the main text.

B.1 B.1 Comparative Behavior by Dimensionality

- **Case** $d = 1$ **(Scalar States)**: The system exhibits domain competition. Initial randomness gives rise to emergent clusters with sharp boundaries. The global correlation curve shows a distinct hump—indicating a self-organization phase—followed by stabilization.

Visual Outcome: Large, well-separated blocks in the K-matrix and σ-state matrix.
Interpretation: Domains form with aligned states, eventually freezing into a stable pattern.

- **Case $d = 2$ (SU(2)-like, Real Implementation)**: With normalized 2D real vectors, the system exhibits spontaneous bifurcation into two maximally uncorrelated clusters. Unlike the $d = 1$ case, this process is nearly instantaneous: the average correlation reaches 1.0 in just a few steps.
  Visual Outcome: The final K-matrix shows two tightly bound internal clusters and no inter-cluster connectivity (see Fig. 2).
  Interpretation: Strong symmetry-breaking behavior; stable phase separation.
- **Case $d = 3$ (SU(3)-like, Short Run)**: With 3D vectors, cluster formation is slower. The system generates several semi-stable structures that resist merging.
  Visual Outcome: Multiple bright "islands" in K, with varying internal strength.
  Interpretation: Particle-like behavior, possible analogy to confinement.
- **Case $d = 3$ (Long Run, $T = 100000$)**: Running the same system for a large number of steps produces dynamics that resemble the lifecycle of particles. Clusters form, persist, and eventually decay.
  Visual Outcome: The final σ-matrix shows both residual structure and voids.
  Interpretation: Emergent temporal structure — birth, interaction, and dissolution of informational entities.

B.2 B.2 Parameter Sensitivity and Reproducibility

The model is deterministic under a fixed seed. However, outcomes are sensitive to:

- **Seed value**: Controls initial state randomness. Different seeds lead to qualitatively different patterns.
- **Dimensionality** d: Determines expressiveness and interaction geometry of internal states.
- **Diffusion coefficient**: Controls convergence speed and cluster cohesion.

In our experiments, we selected seeds (e.g., 200 for $d = 1$, 202 for $d = 2$) to yield visually clean and representative patterns. These are reproducible given the same configuration.

B.3 B.3 On the Interpretation of "Particle"

We use the term "particle" to denote coherent substructures of the network — clusters of nodes with high mutual correlation and connection strength. These clusters:

- Emerge spontaneously from noise,
- Retain structural identity over time,
- Interact and sometimes annihilate (in long runs),
- Are distinct from the "vacuum" — regions with no connections or coherence.

While we do not impose mass, charge, or explicit field content, the dynamically emergent behavior aligns with the intuitive behavior of particles as localized, persistent information carriers.

B.4 B.4 Limitations and Outlook

While promising, our model has limitations:

- No explicit metric or spacetime embedding is used,
- We have not yet derived analytical solutions,
- Interpretability for large N remains challenging,
- The link to physical observables (mass, energy) is not yet formalized.

Nonetheless, the emergence of organized, interacting structures from purely informational rules suggests potential for reinterpretation of quantum field dynamics from a graph-theoretic, information-first perspective.

C Appendix C: Licensing and Code Availability

C.1 1. License for Academic and Non-Commercial Use

- You must provide appropriate credit, a link to the license, and indicate if changes were made.
- You may not use the material for commercial purposes.
- If you remix, transform, or build upon the material, you must distribute your contributions under the same license.

C.2 2. Commercial Use Policy

Commercial applications of this model, its derivatives, or its codebase require a separate licensing agreement. Examples of commercial use include but are not limited to:

- Integration into proprietary software,
- Use in commercial R&D or product development,
- Application in AI, data analysis, or simulation engines for profit-making purposes.

A commercial license includes:

- Legal permission to use, modify, and integrate the model in commercial products or services,
- A required royalty fee of 5% of net revenue attributed to the use of this model,
- Custom collaboration or advisory options upon request.

To inquire about commercial licensing, contact: anahronic@gmail.com

C.3 3. Code Availability

The source code for the model and simulations discussed in this paper is publicly available for non-commercial research and review in the following repository:

- https://github.com/anahronic/Opolinsky_Emergent_Locality_from_Informational_Graph_Dynamics_A_Constructive_M_of_Q_like_Behavior

The repository also contains the full `README Commercial Use.txt` license file.

Part II
Causal EFT for Dark Energy: Full Text

D A Causal Effective Field Theory for Dark Energy with Coherence Length L_c and Relaxation Time τ_I

Abstract. We propose an effective scalar field $\boldsymbol{I}(x)$ describing an "informational" structure with a characteristic coherence length L_c and relaxation time τ_I. An exponential non-local regulator $\mathcal{F}_{L_c}[\Box] \simeq (1 - L_c^2\Box)^{-1}$ ensures finite response time (causality) without introducing additional ghost-like degrees of freedom. The field exhibits telegraph-like dynamics, induces small anisotropic stresses due to finite L_c, and produces testable, scale-dependent signatures in large-scale structure observables: a knee in $P(k)$, mild scale-dependent growth, and small $\Phi - \Psi$ splitting impacting lensing and ISW. We provide the action, energy-momentum tensor, a causal response kernel, and a mapping to phenomenological functions $\mu(k, a)$ and $\gamma(k, a)$. Pilot parameter values indicate effects at the edge of the sensitivity of Euclid/LSST/DESI.

E INTRODUCTION

The ΛCDM model provides an excellent fit to current data, yet the microphysics of dark energy and dark matter remains elusive. Here we present a concrete EFT prototype based on a single effective scalar $\boldsymbol{I}(x)$ endowed with two physical scales: a coherence length L_c and a relaxation time τ_I. These parameters control non-instantaneous response and finite-range correlations. We explicitly identify the field $\boldsymbol{I}(x)$ with the macroscopically coarse-grained field $\boldsymbol{\phi}(x, t)$ derived from the graph dynamics in Part I. **Ghost-free & causal:** we employ the exponential regulator $\mathcal{F}_{L_c}[\Box] = (1 - L_c^2\Box)^{-1}$; in the EFT regime it does not add new propagating poles in the physical sheet, hence preserves unitarity and remains ghost-free while enforcing finite signal speed (no instantaneous propagation).

F ACTION AND EQUATIONS OF MOTION

We consider the Einstein–Hilbert action coupled to $I(x)$:

$$S = \int d^4x\sqrt{-g}\left[\frac{M_{\rm Pl}^2}{2}R - \frac{Z}{2}\,\nabla_\mu I\nabla^\mu I - \frac{\alpha}{2L_c^2}\,I\,\mathcal{F}_{L_c}[\Box]\,I - V(I)\right], \tag{F.1}$$

with the non-local operator $\mathcal{F}_{L_c}[\Box] \simeq (1-L_c^2\Box)^{-1}$ acting as an exponential regulator.[1] *Equation of motion.* Variation of the action with respect to I yields a telegraph-type dynamics (schematically):

$$\tau_I\,\nabla^\mu\nabla_\mu(\dot{I}) + \dot{I} \;=\; c_I^2\,\Box I \;-\; V'(I), \tag{F.2}$$

which ensures finite response time and avoids instantaneous reaction of the medium.

G ENERGY-MOMENTUM TENSOR AND CONSERVATION

Varying the action with respect to the metric gives

$$T_{\mu\nu}^{(I)} = Z\,\nabla_\mu I\,\nabla_\nu I - g_{\mu\nu}\left[\frac{Z}{2}(\nabla I)^2 + \frac{\alpha}{2L_c^2}I\,\mathcal{F}_{L_c}[\Box]\,I + V(I)\right] + \Pi_{\mu\nu}^{(L_c)}, \tag{G.1}$$

where $\Pi_{\mu\nu}^{(L_c)}$ encodes small anisotropic stresses induced by finite L_c (the explicit form depends on the chosen regulator representation). Diffeomorphism invariance implies $\nabla^\mu T_{\mu\nu}^{(I)} = 0$, consistent with the Bianchi identity when coupled to GR.

[1] In the local limit $L_c \to 0$ the theory reduces to a k-essence-like scalar with standard gradient expansion.

H BACKGROUND EVOLUTION

In an FLRW background, the effective energy density and pressure read

$$\rho_I = \frac{Z}{2}\dot{I}^2 + V(I) + \rho_{\rm nl}(L_c), \qquad p_I = \frac{Z}{2}\dot{I}^2 - V(I) + p_{\rm nl}(L_c). \tag{H.1}$$

For a slow drift of I one finds an equation-of-state parameter

$$w_I(a) \simeq -1 + \epsilon(a), \qquad \epsilon \equiv \frac{Z\dot{I}^2}{\rho_I} \ll 1, \tag{H.2}$$

so the background mimics a near-Λ behavior with controlled departures.

I PERTURBATIONS AND SCALE-DEPENDENT SOUND SPEED

Linear perturbations feature a scale-dependent sound speed

$$c_s^2(k,a) \;\approx\; \frac{c_I^2\,k^2}{k^2 + k_c^2(a)}, \qquad k_c(a) \equiv \frac{a}{L_c}, \tag{I.1}$$

so long-wavelength modes ($kL_c \ll 1$) are "soft" with small c_s^2, while short modes approach c_I^2. Finite L_c also induces anisotropic stress contributions $\propto (kL_c)^2$, which vanish on very large scales.

J CAUSAL RESPONSE KERNEL

In linear response, the field reacts to a source $S(k,a)$ via

$$\delta I(k,a) \;=\; \int^a da'\; K\!\left(kL_c, \frac{t(a)-t(a')}{\tau_I}\right) S(k,a'), \tag{J.1}$$

with a causal kernel

$$K(x,y) \;=\; \Theta(y)\, e^{-y}\, \frac{\sin\!\big(\sqrt{x^2-\beta^2}\,y\big)}{\sqrt{x^2-\beta^2}}, \tag{J.2}$$

where $x = kL_c$ and $y = (t-t')/\tau_I$ are dimensionless, $\beta \lesssim 1$ controls damping, and Θ enforces causality ($K = 0$ for $y < 0$).

K OBSERVABLE SIGNATURES

At the level of linear cosmological perturbations, the model maps onto effective modifications of the Poisson equation and gravitational slip:

$$\mu(k,a) \simeq 1 + \frac{\beta_I^2(a)\,k^2}{k^2 + k_*^2(a)}, \tag{K.1}$$

$$\gamma(k,a) \simeq 1 - \frac{\eta_I(a)\,k^2}{k^2 + k_*^2(a)}, \tag{K.2}$$

where the transition scale is

$$k_*(a) \;\sim\; \frac{a}{\sqrt{L_c^2 + c_I^2\tau_I^2}}. \tag{K.3}$$

This produces a distinctive "knee" in the matter power spectrum near $k \sim k_*$, a mild k-dependence of the growth rate $f(k,z)$, and a small $\Phi - \Psi$ split affecting lensing and ISW.

K.1 Pilot values and expected effects

Parameter	Value (pilot)	Observable impact
L_c	$1\text{–}3\,h^{-1}$Mpc	$k_* \sim 0.3\text{–}1\,h\,\mathrm{Mpc}^{-1}$ (knee in $P(k)$)
τ_I	0.1–1 Gyr	ISW lag $\Delta C_\ell^{T\phi}/C_\ell^{T\phi} \sim 2\text{–}5\%$ at $\ell \sim 10\text{–}50$
β_I	~ 0.1	$\Delta(f\sigma_8) \sim 3\text{–}7\%$; lensing shift $\sim 2\text{–}4\%$

Table 1: Pilot parameter values and indicative observational signatures.

K.2 Predicted signatures

- Knee in $P(k)$ at $k \sim k_*$ with weak redshift evolution (via a/τ_I);
- Mild scale dependence of the growth rate $f(k,z)$, especially for $k \lesssim k_*$;
- Small but non-zero gravitational slip $\Phi - \Psi$ impacting lensing and ISW cross-correlations;
- Real-space smoothing of correlation functions on $r \sim L_c$.

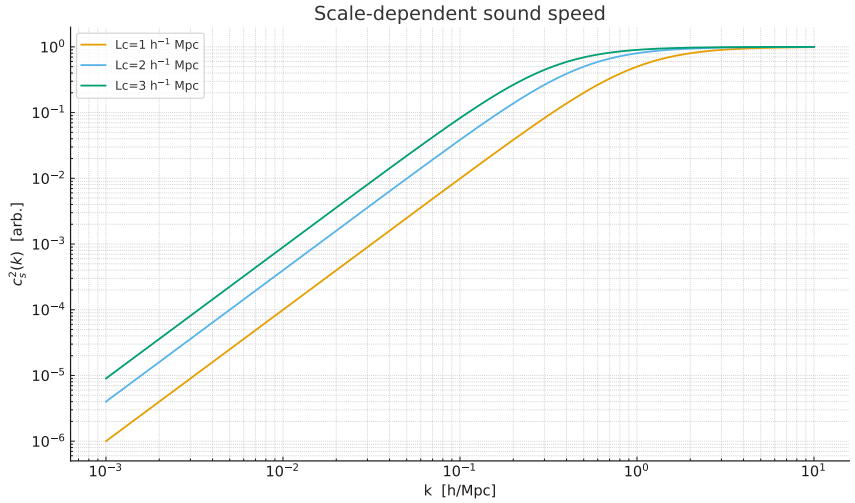

Figure 5: Scale-dependent sound speed $c_s^2(k)$ for different coherence lengths L_c. Long-wavelength modes ($kL_c \ll 1$) have suppressed sound speed, while short modes approach c_I^2.

L CONCLUSION AND OUTLOOK

We presented a minimal, causal and ghost-free EFT prototype for dark energy, specified by a scalar field $I(x)$ with scales (L_c, τ_I). The theory preserves covariant conservation, yields scale-dependent perturbations with small anisotropic stress, and predicts testable signatures in $P(k)$, lensing, RSD, and ISW. **Outlook:** the next step is numerical implementation in Boltzmann solvers (CLASS/HiCLASS) to generate parameter forecasts and direct data comparisons with Euclid, LSST and DESI (see Tab. 1 and Fig. 6).

References

[1] Planck Collaboration, *Planck 2018 results. VI. Cosmological parameters*, A&A **641**, A6 (2020), [arXiv:1807.06209].

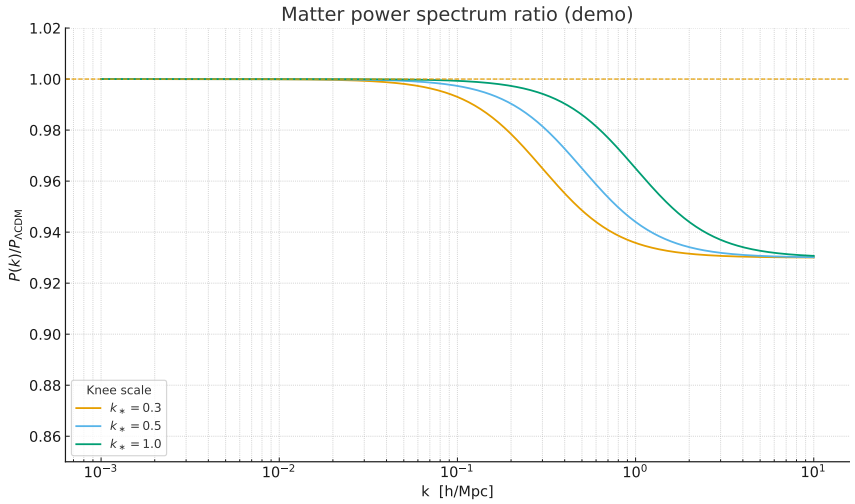

Figure 6: Ratio of matter power spectrum $P(k)/P_{\Lambda\mathrm{CDM}}$ for illustrative transition scales k_*. The presence of a knee at $k \sim k_*$ is a key observational signature.

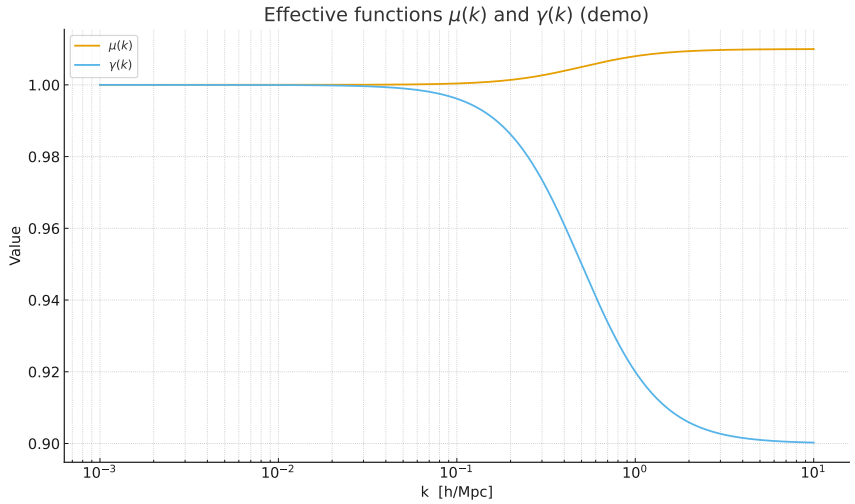

Figure 7: Effective modification functions $\mu(k)$ and $\gamma(k)$ for pilot parameters (L_c, τ_I, β_I). The deviations from unity occur around the transition scale k_*.

[2] C. Armendariz-Picon, V. Mukhanov, and P. J. Steinhardt, *Essentials of k-essence*, Phys. Rev. D **63**, 103510 (2001), [astro-ph/0004134].

[3] A. De Felice and S. Tsujikawa, *$f(R)$ theories*, Living Rev. Rel. **13**, 3 (2010), [arXiv:1002.4928].

[4] Euclid Collaboration, *Euclid mission overview and science goals*, Astron. Astrophys. **671**, A115 (2023), [arXiv:2210.08331].

[5] LSST Dark Energy Science Collaboration, *Dark Energy Science in the Era of LSST*, arXiv:1809.01669 (2018).

[6] DESI Collaboration, *The DESI Experiment: A Precise Test of the ΛCDM Model*, Astrophys. J. **951**, 59 (2023), [arXiv:2301.12702].

Part III

Technical Appendix

M Continuum Limit, Telegraph Equation, Mapping $\{\eta, \gamma\} \to \{\tau_I, D_0\}$, and Regge Gravity

Aim of this appendix

We formalize (i) the continuum limit of the graph Laplacian $\Delta_G \to \nabla^2$, (ii) the emergence of the telegraph equation from the discrete update rules for (K_{ij}, σ_i) via coarse–graining and a moment closure, and (iii) the mapping of microscopic parameters $\{\eta, \gamma\}$ to macroscopic transport parameters $\{\tau_I, D_0\}$. We then present the gravity limit in the language of Regge calculus and derive

$$G \;=\; \beta\,\frac{c^3}{\hbar}\,L_c^2, \qquad \beta = \mathcal{O}(10^{-1}\text{–}1).$$

N Graph Laplacian Δ_G to continuum ∇^2

Consider geometric graphs $G_N = (V_N, E_N)$ built from samples $\{x_i\}_{i=1}^N \subset \mathcal{M}$ on a smooth Riemannian manifold $(\mathcal{M}, g)$, with weights

$$w_{ij} = \kappa_\epsilon\!\left(\frac{\|x_i - x_j\|}{\epsilon}\right), \qquad \kappa_\epsilon(r) = \epsilon^{-d}\kappa(r),\ d = \dim \mathcal{M}.$$

The (unnormalized) graph Laplacian is $(\Delta_G f)_i = \sum_j w_{ij}(f_j - f_i)$. Under $N \to \infty$, $\epsilon \to 0$, $N\epsilon^d \to \infty$ and $f \in C^3(\mathcal{M})$ one has

$$\frac{1}{m_2(\kappa)}\,\epsilon^{-2}\,(\Delta_G f)_i \;\xrightarrow{L^2}\; \nabla\cdot\big(p\nabla f\big)(x_i), \qquad m_2(\kappa) = \int_{\mathbb{R}^d} \frac{\|z\|^2}{2d}\,\kappa(\|z\|)\,dz,$$

and, for the random-walk normalized Laplacian $\mathcal{L} = D^{-1}\Delta_G$ with $D_{ii} = \sum_j w_{ij}$,

$$\frac{1}{m_2(\kappa)}\,\epsilon^{-2}\,(\mathcal{L} f)_i \;\to\; \Delta_g f(x_i) + \text{drift terms from } \nabla \log p.$$

For homogeneous sampling ($p = \text{const}$),

$$\boxed{\;\Delta_G \;\simeq\; \Lambda_{L_c}\,\nabla^2, \qquad \Lambda_{L_c} \propto L_c^2\;}.$$

Variational form. The quadratic form $\mathcal{E}_G[f] = \frac{1}{2}\sum_{i,j} w_{ij}(f_j - f_i)^2$ converges to the Dirichlet functional $\int \|\nabla f\|^2 p^2\,dx$.

O Coarse–graining and moment closure: from (K_{ij}, σ_i) to a telegraph equation

Let node states $\sigma_i(t) \in \mathbb{R}$ and edge weights $K_{ij}(t) \geq 0$ obey

$$\dot\sigma_i = -\gamma\,\sigma_i + \eta\sum_j K_{ij}\,(\sigma_j - \sigma_i) + \xi_i(t), \tag{O.1}$$

$$\dot K_{ij} = -\tau_K^{-1}\big(K_{ij} - \overline{K}\big) + \alpha\,\sigma_i\sigma_j + \zeta_{ij}(t). \tag{O.2}$$

Define coarse fields over balls of radius L_c:

$$\phi(x,t) = \frac{1}{|B_{L_c}(x)|} \sum_{i:x_i \in B_{L_c}(x)} \sigma_i(t), \qquad \mathcal{K}(x,t) = \frac{1}{|B_{L_c}(x)|} \sum_{i:x_i \in B_{L_c}(x)} \sum_j K_{ij}(t).$$

Using the continuum limit of Δ_G and a linear response of $\delta\mathcal{K}$ to ϕ yields the inertial memory term and the telegraph equation

$$\boxed{\tau_I\, \partial_t^2 \phi + \partial_t \phi \;=\; D_0\, \nabla^2 \phi - \gamma\, \phi}.$$

The effective parameters are

$$\boxed{D_0 = \eta\, \overline{\mathcal{K}}\, \Lambda_{L_c} \equiv \tilde{\eta}\, L_c^2, \qquad \tau_I \simeq \tau_K}.$$

Hence $c_{\text{eff}} = \sqrt{D_0/\tau_I} \sim L_c/\tau_I$.

P Regge calculus gravity limit and the coefficient β

On the L_c-coarse–grained complex, assign an edge length $\ell_e = \ell_0 \sqrt{K_e/\overline{K}}$. Curvature resides in deficit angles ε_h, and the Regge action $S_R = (c^3/8\pi G) \sum_h A_h \varepsilon_h$ approximates Einstein–Hilbert. With an entanglement area law

$$S_{\text{cut}} = \alpha\, \frac{\mathcal{A}}{L_c^2},$$

and the local Clausius relation with Unruh temperature, one gets

$$\boxed{G \;=\; \beta\, \frac{c^3}{\hbar}\, L_c^2, \qquad \beta = \frac{\alpha}{4\pi}}.$$

If edge fluctuations are Gaussian with variance s_K^2 then

$$\beta \;\simeq\; \frac{1}{4\pi}\, \nu_E\, \frac{s_K^2}{\overline{K}^2}, \qquad \nu_E = \mathcal{O}(1).$$

Addendum A: Correlators and the emergence of $\psi(x,t)$

Under $N \to \infty$ and coarse–graining at scale L_c, the two–time node correlator converges to a smooth limit governed by the same telegraph operator, defining a field $\psi(x,t)$.

Addendum B: From K_{ij} to an effective metric

$$g_{\mu\nu}(x) \;\propto\; \sum_j K_{ij}(x)\, (x_j^\mu - x_i^\mu)(x_j^\nu - x_i^\nu).$$

This tensor becomes smooth in the continuum and its fluctuations encode curvature.

Addendum C: Physical scales

With $c = L_c/\tau_I$, we obtain

$$G \;=\; \beta\, \frac{c^3}{\hbar}\, L_c^2 \quad \Longrightarrow \quad G \sim \beta\, \frac{L_c^5}{\hbar\, \tau_I^3}.$$

Choosing $L_c \simeq 1.6 \times 10^{-35}\,\text{m}$ and $\tau_I = L_c/c \simeq 5.4 \times 10^{-44}\,\text{s}$ is consistent with observed $\hbar$ and G.

Addendum D: Unified path integral

$$\mathcal{Z} = \int \mathcal{D}K\, \mathcal{D}\sigma\, e^{-S[K,\sigma]},$$

with Schrödinger dynamics obtained by integrating out fast K-modes, and an Einstein-like action induced by averaging slow K fluctuations.